Supplementary information appendix to the manuscript:

Secretagogin marks amygdaloid PKCδ interneurons and modulates NMDA receptor availability

Zsófia Hevesi, Dóra Zelena, Roman Romanov, János Hanics, Attila Ignácz, Alice Zambon, Daniela Pollak, Dávid Lendvai, Katalin Schlett, Miklós Palkovits, Tibor Harkany, Tomas G.M. Hökfelt and Alán Alpár

This file contains

Supplementary figures 1-6,
Supplementary tables 1-2,
Legends to supplementary figures and table,
Supplementary materials and methods,
Supplementary references.

Supplementary figures

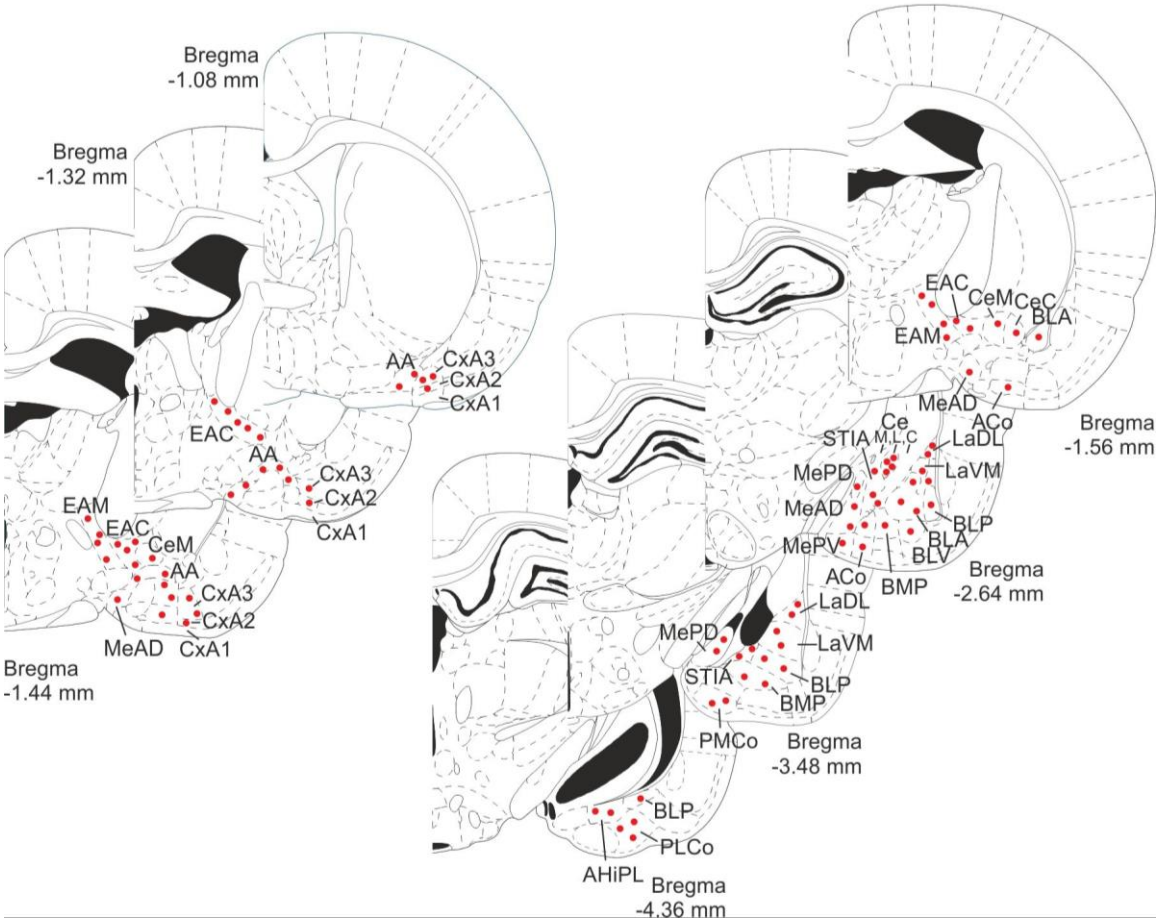

Figure S1. Brain-wide mapping of Scgn⁺ neurons in the amygdaloid complex of the rat. Neurons were identified by anti-Scgn immunohistochemistry. Systematic brain mapping revealed Scgn⁺ neurons in most amygdaloid regions (*red circles*). *Abbreviations:* AA, anterior amygdaloid area; ACo, anterior cortical amygdaloid nucleus; AHiPL, amygdalohippocampal area, posterolateral part; BLA, basolateral amygdaloid nucleus, anterior part; BLP, basolateral amygdaloid nucleus, posterior part; BLV, basolateral amygdaloid nucleus, ventral part; BMP, basomedial amygdaloid nucleus, posterior part; CeC, central amygdaloid nucleus, capsular part; CeL, central amygdaloid nucleus, lateral division; CeM, central amygdaliod nucleus, medial division; CxA1-CxA3. cortex-amygdala transition zones, layers 1-3; EAC, sublenticular extended amygdala, central part; EAM, sublenticular extended amygdala, medial part; LaDL, lateral amygdaloid nucleus, dorsolateral part; LaVM, lateral amygdaloid nucleus, ventromedial part; MeAD, medial amygdaloid nucleus, ant dorsal; MePD, medial amygdaloid nucleus, posterodorsal part; MePV, medial amygdaloid nucleus, posteroventral part; PLCo, posterolateral cortical amygdaloid nucleus; PMCo, posteromedial cortical amygdaloid nucleus; STIA, bed nucleus of stria terminalis, intraamygdaloid division.

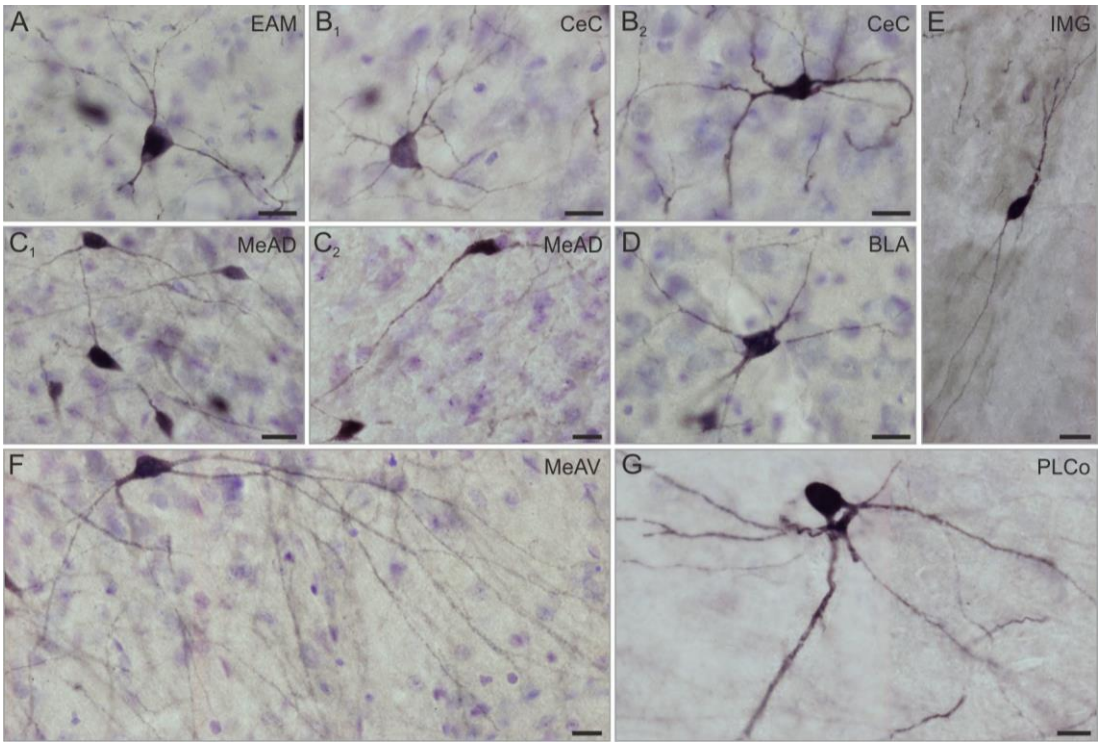

Figure S2. Scgn$^+$ neurons are typically of multipolar or fusiform types. Somata and dendritic arbors were visualized by anti-Scgn immunohistochemistry. Multipolar neurons (A, B_1, B_2, C_1, D, F, G) had dendritic arbors with smooth dendritic sections that could be traced over 100 µm-s in several cases (f). Bipolar, fusiform neurons had an ovoid cell body and elongated dendritic trees emanated from opposite poles of the soma (C_2, E). *Abbreviations:* BLA basolateral amygdaloid nucleus, anterior part; CeC central amygdaloid nucleus, capsular part; EAM sublenticular extended amygdala, medial part; IMG amygdaloid intramedullary gray; MeAD medial amygdaloid nucleus, ant dorsal; MeAV medial amygdaloid nucleus, anteroventral part; PLCo posterolateral cortical amygdaloid nucleus. *Scale bars* = 10 µm.

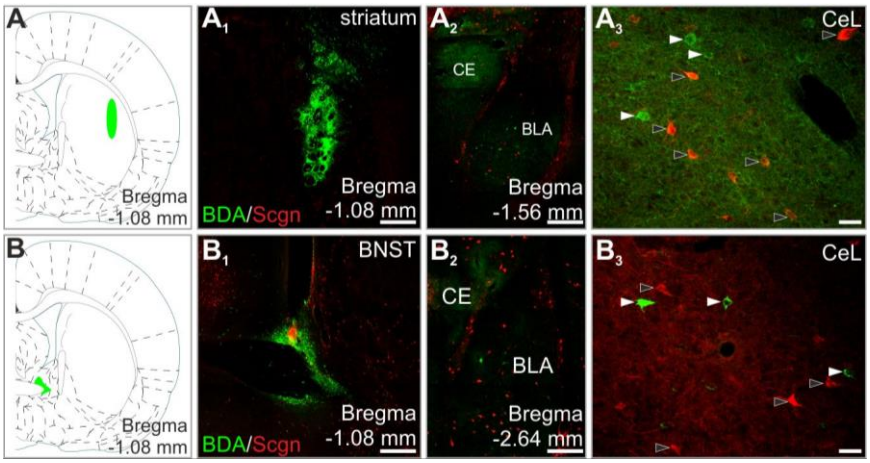

Figure S3. Scgn$^+$ neurons are non-projecting cells. (A-B_3) Retrograde tracing from the striatum and from the bed nucleus of stria terminalis (BNST) did not result in any retrogradely-labelled Scgn$^+$ neuron in the CeL (*white arrowheads* point to BDA$^+$/Scgn$^-$ neurons; *black arrowheads* point to BDA$^-$/Scgn$^+$ neurons in the CeL). *Abbreviations:* BDA, biotinylated dextran amine; BLA basolateral amygdala; CE, central amygdala; CeL centrolateral amygdala. *Scale bars* = 500 µm (A_1,B_1), 300 µm (A_2,B_2), 10 µm (A_3,B_3).

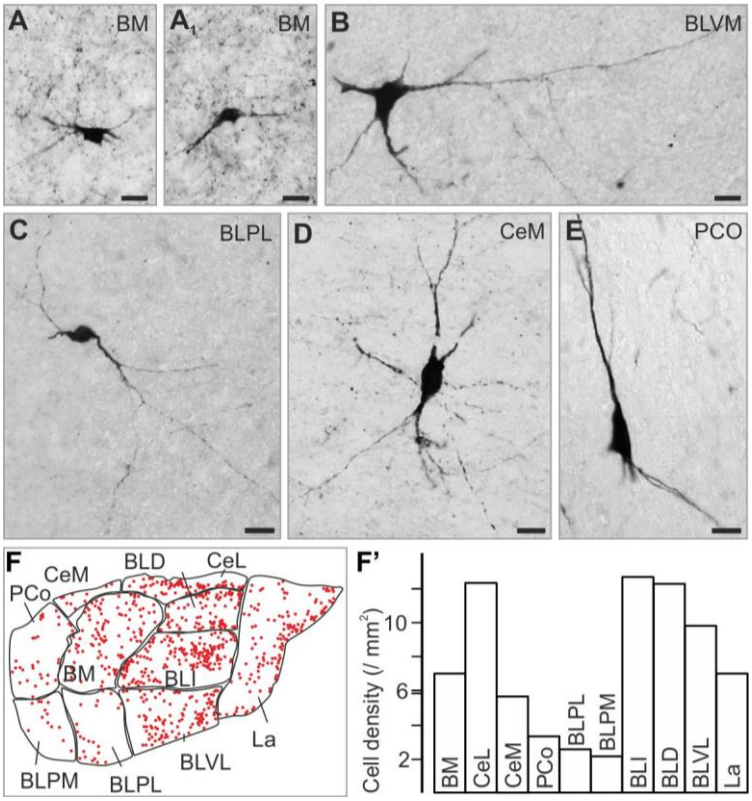

Figure S4. Scgn⁺ neurons in the human amygdala. Somata and dendritic arbors were visualized by anti-Scgn immunohistochemistry. (A,B,D) Multipolar neurons were seen in different divisions of the human amygdala. (A_1,C,E) Bipolar neurons expressed Scgn less frequently. (F,F') Distribution map of Scgn⁺ neurons in the caudal portion of the human amygdala. *Abbreviations*: BM, basomedial amygdaloid nucleus; BLD, basolateral amygdaloid nucleus, dorsal part; BLI, basolateral amygdaloid nucleus, inferior part; BLPM, basolateral amygdaloid nucleus, posteromedial part; BLPL, basolateral amygdaloid nucleus, posterolateral part; BLVM, basolateral amygdaloid nucleus, ventromedial part; BLVL basolateral amygdaloid nucleus, ventrolateral part; BM, basomedial amygdaloid nucleus; CeM, central amygdaloid nucleus, medial division; CeL, central amygdaloid nucleus, lateral division; La, lateral amygdaloid nucleus; PCo, posterior cortical amygdaloid nucleus. *Scale bars* = 15 µm (A-E).

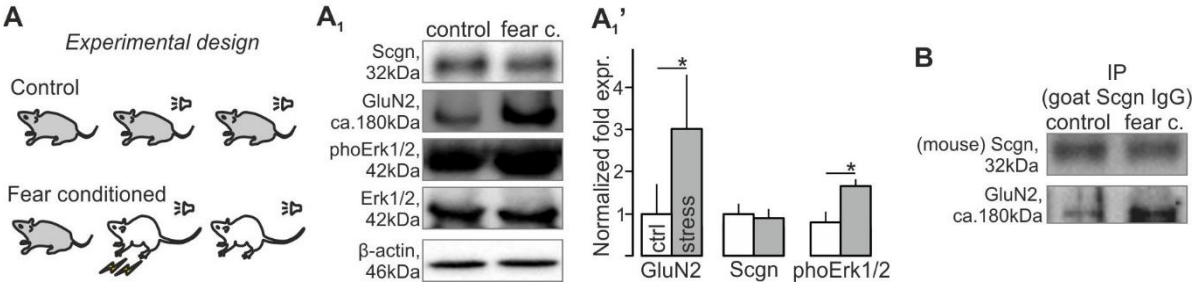

Figure S5. Protein expression and interaction changes in the applied fear conditioning paradigm. (A-A_1') In the applied danger avoidance behavioural paradigm, commonly termed "fear conditioning", we reproduced – and validated for the present study - increased protein levels of GluN2A/B and enhanced Erk1/2 phosphorylation locally) (1, 2). (B) Fear conditioning increased the amount of immunoprecepitated GluN2 when using secretagogin antibody in rat amygdala homogenate. (A_1') $p < 0.05$, Student's *t*-test. *Abbreviations* ctrl control; GluN2 glutamate receptor subunit type 2; Scgn secretagogin.

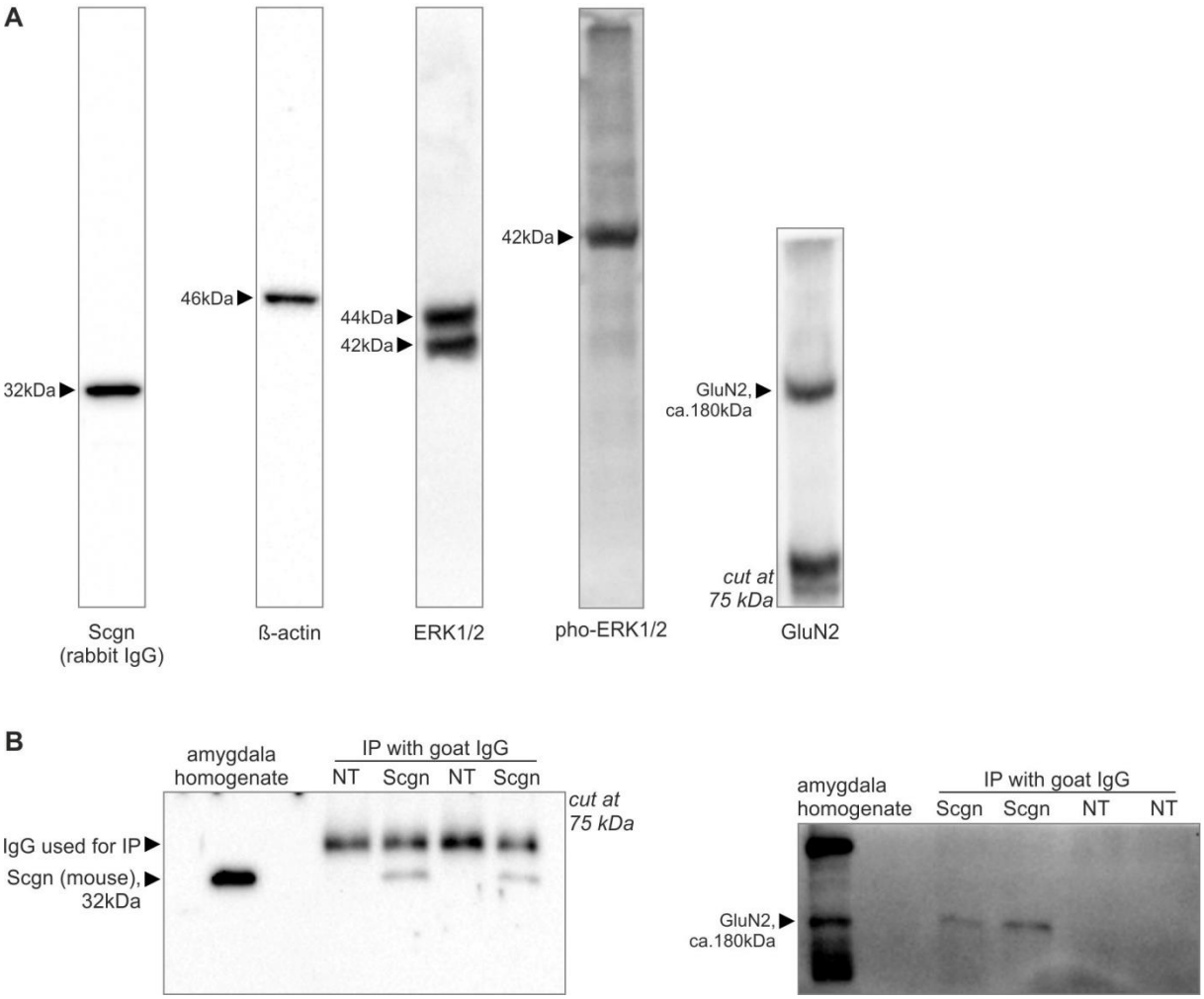

Figure S6. Full lanes of Western blots immunoprecipitation experiments. (A) Western blotting. (B) Immunoprecipitation. *Abbreviations*: ERK1/2 extracellular signal-regulated kinase 1/2; GluN2, glutamate receptor subunit type 2; NT, non-target IgG; Scgn, secretagogin.

Supplementary tables

Table S1 – Demography and use of human subjects

Case ID	**Status**	**Age** (y)	**Gender**	**Analysis**
#KF1	control	83	female	IHC
#KF2	control	79	male	IHC

Supplementary tables

Table S2 – List of markers used for immunolabelling

Marker	Source	Host	IH dilution	WB dilution	Reference
β-actin	Sigma	Mouse, mc[1]	n.a	1:10,000	Lendvai *et al.*, 2013
Biotinylated dextran amine, 10 kDa	Molecular Probes	n.a.	n.a.	n.a.	Alpár *et al.*, 2018
c-fos	Santa Cruz	Rabbit, pc[2]	1:7,500	n.a.	Renner *et al.*, 2012
ERK1/2	Cell Signaling	Rabbit, pc[2]	n.a.	1:2000	Alpár *et al.*, 2018
GluN2A/B	Synaptic Systems	Rabbit, pc[2]	1:250	1:1000	Gut *et al.*, 2013
pho-ERK1/2	Cell Signaling	Rabbit, pc[2]	1:1,000	n.a.	Alpár et al., 2018
pho-GluN2B (Tyr-1472)	Cell Signaling	Rabbit, pc[2]	n.a.	1:1,000	this study
PKCδ	BD Biosci	Mouse, mc[1]	1:1,000	n.a.	Hua *et al.*, 2018
PSD-95	Sigma	Mouse, mc[1]	n.a.	1:2,000	Bullmann *et al.*, 2016
Secretagogin	L.Wagner	Rabbit, pc[2]	1:12,000	1:12,000	Romanov *et al.*, 2015
Secretagogin	R&D Systems	Goat, pc[2]	1:100	1:1,000	Mulder *et al.*, 2010
Synaptophysin	Synaptic Systems	Rabbit, pc[2]	n.a.	1:5,000	Alpár *et al.*, 2014

[1]monoclonal antibody, [2]polyclonal antibody

Supplementary materials and methods

***In situ* fixed human samples.** For light microscopy, human tissues were collected at necropsy from patients at the Second Department of Pathology, Semmelweis University (Budapest, Hungary, TUKEB 84/2014, **Table S1**). The quality at which the (sub-)cellular structure of *post-mortem* brain tissues is preserved impacts the sensitivity and spatial resolution of immunohistochemistry at the light- and electron microscopy levels. The variable *post-mortem* delay and particularly paraformaldehyde (PFA) penetration of blocked tissues during *immersion* fixation pose major challenges. Therefore, we have applied direct PFA perfusion *via* the internal carotid and vertebral arteries, which facilitated the preservation of tissue integrity relative to alternative fixation methods. The removal and subsequent preparation of human tissues were in accordance with relevant ethical guidelines of Semmelweis University (1998). Human brains (n = 2) were perfused with physiological saline followed by a fixative containing 2% PFA and 1% glutaraldehyde in 0.1 M Tris-buffered saline (TBS, pH 7.4) 5h or 18h after death. The amygdala was dissected out of both hemispheres, post-fixed in 2% PFA in TBS for 72h, followed by immersion in cryoprotective sucrose (30%; in 0.1M phosphate buffer (PB, pH 7.4)) overnight. Coronal sections (40 µm) were cut on a cryostat microtome and processed for immunohistochemistry. Amygdala regions were identified according to the Atlas of the Human Brain (3).

***In vivo* tract tracing.** Rats (n = 9) were anesthetized intramuscularly with a mixture of ketamine (50 mg/kg b.w.) and xylazine (4 mg/kg b.w.) and placed in a Kopf stereotaxic instrument. The skull was exposed by a skin incision, and small holes were drilled through the skull. Tracers were injected stereotaxically using a 1.0 µL Hamilton syringe mounted on a Kopf microinjector unit. Biotinylated dextran amine (BDA, 10kDA, Molecular Probes) as a retrograde tracer was deposited into the target brain region (0.1 µL in volume) by slow pressure injection lasting for 5 min. The needle was retracted only after a 15 min resting interval to minimize leakage along the injection canal. Coordinates of target brain regions were verified in pilot experiments by methylene blue injections and based on the brain atlas of Paxinos and Watson (4). Target regions (in n = 3 animals each) included striatum (coordinates from bregma: AP: 0.0 mm, DV: 6 mm, and ML: 3.0 mm), bed nucleus of stria terminalis (AP: -0.24 mm, DV: 6.5 mm, and ML: 1.5 mm) or the nucleus accumbens (AP: 2.04 mm, DV: 6.5 mm, and ML: 1.5 mm) Seven days after surgery, animals were transcardially perfused and their brains processed for immunohistochemistry.

Formalin stress. Rats and received an injection of 4% PFA (50 µl physiological saline) into their right hind paw and subsequently returned to their home cages. After 20 min, the animals were perfused and processed for immunohistochemistry.

Virus delivery *in vivo.* Mice were placed in a stereotaxic frame under isoflurane anesthesia (5%, 1L/min flow rate of tubed air). A Quintessential Stereotaxic Injector (Stoelting) was used to inject virus particles at a speed of 100 nl/min. AAV8-hSyn-DIO-hM4D(Gi)-mCherry (Addgene, #44362), AAV8-hSyn-DIO-hM3D(Gq)-mCherry (Addgene, #44361) or pAAV8-hSyn-DIO-mCherry (Addgene, #50459) was bilaterally injected in the central nucleus of the amygdala (40 nl/side; coordinates from bregma: AP: -1.46 mm, DV: 4.5 mm, L: 2.5 mm) of *Scgn*-Cre mice. The glass pipette (Drummond) was slowly withdrawn 5 min after injection to reduce solution backflow. Twenty to 22 days after viral injections, animals were used for behavioral testing (fear conditioning) and immunohistochemistry to map neuronal connections.

Fear conditioning. Rats were placed into a programmable foot-shock chamber to habituate for 10 min each. Next day, *n* = 6 rats (shocked group) were given five presentations of tone (75dB, 4kHz, 20 sec) co-terminating with foot-shocks (0.6 mA) each during a period of 650 seconds with random intervals ranging from 90 to 120s. Control rats (*n* = 6) received the same series of five tone presentation without foot-shock. On the third day, animals were given only the tone without foot-shock (5, 6) in an altered context (soap was used for cleaning instead of ethanol and the wall of the conditioning box was changed). Animals were then removed from the chamber, decapitated, their amygdala isolated and prepared for Western blotting and immunoprecipitation. EthoVision (Noldus) was used to analyze the following parameters: *(i)* total freezing time, *(ii)* total distance covered in cage and the calculated % of freezing time after fear conditioning, during 650 seconds.

The same experimental protocol was applied to test *Scgn*$^{-/-}$ mice in fear conditioning experiments. A total of 14 mice were used (*n* = 5 KO (*Scgn*$^{-/-}$) mice and *n* = 9 wildtype littermate controls).

Fear conditioning experiments with virus-injected *Scgn*-Cre mice were conducted in an identical fashion. On the second day clozapine N-oxide (Tocris, 1mg/kg b.w.) was injected intraperitoneally 30 min before training to activate DREADD constructs (*see above*) *in vivo*. To avoid any difference due to possible metabolism (7) we used CNO in all animals instead of saline controls. Although AAVs are considered rather safe and do not induce a high immune reaction (8), control animals received control virus instead of including non-injected animals for this purpose. Similar comparison on behaviour between control and stimulatory virus injected mice using the same CNO concentration and timing was already published (9). All mice received the tone-combined foot-shock pairings. Animals were then removed from the chamber and perfused for immunohistochemistry.

Immunohistochemistry. Free-floating rodent sections (30 µm) were rinsed in PB (pH 7.4) and pre-treated with 0.3% Triton-X 100 (Sigma: in PB) at 22 - 24 °C for 1h to enhance the penetration of antibodies (10-19). Non-specific immunoreactivity was reduced by incubating our specimens in a cocktail of 5% normal donkey serum (NDS; Jackson), 2% bovine serum albumin (BSA; Sigma) and 0.3%

Triton X-100 in PB at 22 - 24 °C for 1h. Sections were exposed (16 - 72h at 4 °C) to selected combinations of primary antibodies (**Table S2**) diluted in PB to which 0.1% NDS and 0.3% Triton X-100 had been added. After extensive rinsing in PB, sections were processed by using chromogenic or immunofluorescence detection. In single labelling experiments, hippocampal sections were exposed to biotinylated anti-rabbit IgG raised in donkey (1:1,000 [Jackson], 22 - 24 °C, 2h) followed by pre-formed avidin-biotin complexes also incorporating horseradish peroxidase (1h). Immunosignals were visualized by 3,3'-diaminobenzidine (i0.025%; Sigma,) as chromogen intensified with Ni-ammonium sulphate (0.05%, Merck) in the presence of 0.001% H_2O_2 as substrate (dissolved in 0.05M Tris buffer, pH 8.0). In multiple immunofluorescence labelling experiments, immunoreactivities were revealed by carbocyanine (Cy) 2, 3 or 5-tagged secondary antibodies raised in donkey (1:200 [Jackson], 22 - 24 °C, 2h). Glass-mounted sections were coverslipped with glycerol/gelatin (GG-1; Sigma).

Results of chromogenic stainings were captured on an Olympus BX-51 microscope at 2x, 10x and 20x primary magnification. Sections processed for multiple immunofluorescence histochemistry were inspected and images acquired on a 780LSM confocal laser-scanning microscope (Zeiss) with optical zoom ranging from 1x-to-3x at 63x primary magnification (Plan-Apochromat 63x/1.40), and pinhole settings limiting signal detection (0.5 – 0.7 µm). Emission spectra for each dye were limited as follows: Cy2 (505-530 nm), Cy3 (560-610 nm), and Cy5 (650-720 nm). Multipanel figures were assembled in CorelDraw X7 (Corel Corp.).

To measure the overlap of PKCδ and Scgn immunoreactivity we used images captured at 20× primary magnification. PKCδ$^+$ and Scgn$^+$ somata were labelled with different markers in the ZEN software in three animals in the CeL. Immunoreactive somata were identified and marked in a minimum of four corresponding sections which were consecutive serial 30 µm-thick-sections of a four series-section pool. Labelled cells were counted in the whole nucleus on the section. The occurrence of PKCδ or Scgn immunoreactivity in double-labelled somata was calculated and expressed as average ± SEM. This approach was an investigative method and did not aim to provide accurate results regarding cell numbers/proportions.

Western blotting. Amygdala samples of rats and SHSY-5Y cells were homogenized in TNE buffer containing 0.5% Triton X-100, 1% octyl-β-D-glucopyranoside (Calbiochem), 5 mM NaF, 100 µM Na_3VO_4 and a cocktail of protease inhibitors (Complete™, Roche) by using a sonicator. Cell debris and nuclei were pelleted by centrifugation (800*g*, 4 °C for 10 min). Protein concentrations were determined by Bradford's colorimetric method (20). Samples were diluted to a final protein concentration of 2 µg/µL, denatured in 5x Laemmli buffer, and analysed by SDS-PAGE on 8% or 10% resolving gels. After transferring onto Immobilon-FL polyvinylidene difluoride membranes (Millipore), membrane-bound protein samples were blocked in 3% BSA and 0.5% Tween-20 diluted in TBS for 1.5h, and subsequently exposed to primary antibodies (**Table S2**) at 4 °C overnight. Appropriate combinations of HRP-conjugated secondary antibodies were used for signal detection (Jackson; goat, rabbit or mouse hosts; 1:10,000, 2h). Image acquisition and analysis were performed on a Bio-Rad XRS$^+$ imaging platform.

FRAP microscopy. We used a pCI-SEP_NR2B plasmid (Addgene #23998; (21)) to monitor the surface exposure and dynamics of NMDA receptor subtype 2B (NR2B). This plasmid also contains the coding sequence of a super-ecliptic pHluorin (SEP) to facilitate the study of, e.g., vesicle trafficking during postsynaptic receptor endocytosis (22). Here, SH-SY5Y cells were seeded in glass-bottom Petri dishes at 150.000/cm^2 plating density and transfected with 0.5 µg pCI-SEP_NR2B plasmid DNA using jetPRIME transfection reagent (Polyplus transfection). *Scgn* RNA knock-down was also carried out by using jetPRIME, according to the manufacturer's instruction. Twenty-four hours after transfection, the culture medium was changed to imaging buffer (142 mM NaCl, 5.4 mM KCl, 1.8 mM $CaCl_2$, 1 mM NaH_2PO_4, 25 mM HEPES, 5 mM glucose, 0.8 mM $MgCl_2$; pH 7.4) and the cells were kept at 37°C. Fluorescence recovery of the surface NR2B-SEP signal after photobleaching was monitored on a Zeiss CellObserver system equipped with a Yokogawa CSU-X spinning disk device and a 473 nm Rapp bleaching laser operated by the Firefly2 system. Images were recorded every 5 s for 10 min by using a PlanApochromat 40x/1,4 oil objective, with 2x2 binning. Transfected cells were chosen randomly with a bleaching area selected along the equatorial *z*-axis of the plasma membrane. Image sequences consisted of 10 pre-bleach images, 2 seconds of 15% bleaching laser intensity and 60 images of post-bleach recovery. To determine the initial membrane fluorescence, *z*-stack images were taken from live cells at identical imaging settings right before time-lapse imaging had commenced. Average NR2B-SEP signal intensities were measured in a single optical slice in focus next to the nucleus, using FIJI software. Average fluorescence intensities during post-bleach fluorescence recovery were compared at each time point using the IBM SPSS software package. After determining data distribution by the Shapiro-Wilk test, 2-tailed *t*-test was used to compare normally distributed and, alternatively, the Mann-Whitney test to compare non-normally distributed data. For FRAP experiments, n = 10 control and n = 9 $Scgn^{KD}$ cells were used from 2 independent transfection experiments. Baseline membrane intensity was measured in n = 15 control and n = 8 $Scgn^{KD}$ cells.

Imaging under changing pH conditions. SH-SY5Y cells were plated onto PDL-coated wells and grown in DMEM/F12 containing 10% FBS. One day after plating, cells were transferred into DMEM/F12 also containing 1% FBS and 10 µM retinoic acid (Sigma; R2625) for 6 h and subsequently transfected by pCI-SEP_NR2B plasmid DNA (n = 3 wells) or co-transfected with *Scgn* siRNA (n = 3 wells) as above. After 24 h, plates were mounted onto an EVOS FL Auto 2 Microscope (ThermoFisher) equipped with an on-stage incubator and the medium changed to a physiological solution containing 130 mM NaCl, 5.4 mM KCl, 1 mM $MgSO_4$, 1 mM NaH_2PO_4, 1 mM $CaCl_2$, 5 mM glucose and 25 mM HEPES at pH7.4. Images were taken from wells using a 40x lens. Subsequently, cells were kept in an acidic solution (pH 6.0, 130 mM NaCl, 5.4 mM KCl, 1 mM $MgSO_4$, 1 mM NaH_2PO_4, 1 mM $CaCl_2$, 5 mM glucose and 25 mM **4-morpholineethanesulfonic acid**, followed by imaging after 3 min. Finally, the medium was changed to a solution containing 80 mM NaCl, 5.4 mM KCl, 1 mM $MgSO_4$, 1 mM NaH_2PO_4, 1 mM $CaCl_2$, 5 mM glucose, 25 mM HEPES and NH_4Cl at pH7.4 and images were acquired after 5 min.

Supplementary references

1. Sweatt JD (2004) Mitogen-activated protein kinases in synaptic plasticity and memory. *Curr Opin Neurobiol* 14(3):311-317.
2. Bartlett TE & Wang YT (2013) The intersections of NMDAR-dependent synaptic plasticity and cell survival. *Neuropharmacology* 74:59-68.
3. Mai JK (2016) *Atlas of the Human Brain* (Academic Press, New York) Fourth Edition Ed.
4. Paxinos & Watson (1998) *The rat brain in stereotaxic coordinates* (Academic Press, San Diego).
5. Gewirtz JC & Davis M (2000) Using pavlovian higher-order conditioning paradigms to investigate the neural substrates of emotional learning and memory. *Learn Mem* 7(5):257-266.
6. Dalton GL, Wu DC, Wang YT, Floresco SB, & Phillips AG (2012) NMDA GluN2A and GluN2B receptors play separate roles in the induction of LTP and LTD in the amygdala and in the acquisition and extinction of conditioned fear. *Neuropharmacology* 62(2):797-806.
7. Manvich DF*, et al.* (2018) The DREADD agonist clozapine N-oxide (CNO) is reverse-metabolized to clozapine and produces clozapine-like interoceptive stimulus effects in rats and mice. *Sci Rep* 8(1):3840.
8. Zelena D, Demeter K, Haller J, & Balazsfi D (2017) Considerations for the use of virally delivered genetic tools for in-vivo circuit analysis and behavior in mutant mice: a practical guide to optogenetics. *Behav Pharmacol* 28(8):598-609.
9. Szonyi A*, et al.* (2019) Median raphe controls acquisition of negative experience in the mouse. *Science* 366(6469).
10. Bullmann T*, et al.* (2016) Tau phosphorylation-associated spine regression does not impair hippocampal-dependent memory in hibernating golden hamsters. *Hippocampus* 26(3):301-318.
11. Alpár A*, et al.* (2014) Endocannabinoids modulate cortical development by configuring Slit2/Robo1 signalling. *Nature Communications* 5.
12. Lendvai D*, et al.* (2013) Neurochemical mapping of the human hippocampus reveals perisynaptic matrix around functional synapses in Alzheimer's disease. *Acta Neuropathol* 125(2):215-229.
13. Mulder J*, et al.* (2010) Secretagogin is a Ca2+-binding protein identifying prospective extended amygdala neurons in the developing mammalian telencephalon. *Eur J Neurosci* 31(12):2166-2177.
14. Romanov RA*, et al.* (2015) A secretagogin locus of the mammalian hypothalamus controls stress hormone release. *EMBO J* 34(1):36-54.
15. Hanics J*, et al.* (2017) Secretagogin-dependent matrix metalloprotease-2 release from neurons regulates neuroblast migration. *Proc Natl Acad Sci U S A* 114(10):E2006-E2015.
16. Hua R, Yu S, Liu M, & Li H (2018) A PCR-Based Method for RNA Probes and Applications in Neuroscience. *Front Neurosci* 12:266.
17. Alpar A*, et al.* (2018) Hypothalamic CNTF volume transmission shapes cortical noradrenergic excitability upon acute stress. *EMBO J*.
18. Renner E, Puskas N, Dobolyi A, & Palkovits M (2012) Glucagon-like peptide-1 of brainstem origin activates dorsomedial hypothalamic neurons in satiated rats. *Peptides* 35(1):14-22.
19. Gut IM*, et al.* (2013) Novel application of stem cell-derived neurons to evaluate the time- and dose-dependent progression of excitotoxic injury. *PLoS One* 8(5):e64423.
20. Bradford MM (1976) A rapid and sensitive method for the quantitation of microgram quantities of protein utilizing the principle of protein-dye binding. *Anal Biochem* 72:248-254.
21. Kopec CD, Li B, Wei W, Boehm J, & Malinow R (2006) Glutamate receptor exocytosis and spine enlargement during chemically induced long-term potentiation. *J Neurosci* 26(7):2000-2009.

22. Ashby MC, Ibaraki K, & Henley JM (2004) It's green outside: tracking cell surface proteins with pH-sensitive GFP. *Trends Neurosci* 27(5):257-261.